Proc. of SPIE Vol. 1690, Design of Optical Instruments, ed. D M Aikens, V L Genberg, G C Krumweide, M J Thomas (Sep 1992) Copyright SPIE

Structural Design and Analysis for an Ultra Low CTE Optical Bench for the Hubble Space Telescope Corrective Optics

Douglas C. Neam
John D. Gerber
Ball Electro-Optics/Cryogenics Division, Ball Corporation
P.O. Box 1062, Boulder, Colorado 80306

ABSTRACT

The stringent stability requirements of the Corrective Optics Space Telescope Axial Replacement (COSTAR) necessitates a Deployable Optical Bench (DOB) with both a low CTE and high resonant frequency. The DOB design consists of a monocoque thin shell structure which marries metallic machined parts with graphite epoxy formed structure. Structural analysis of the DOB has been integrated into the laminate design and optimization process. Also, the structural analytical results are compared with vibration and thermal test data to assess the reliability of the analysis.

1. INTRODUCTION

COSTAR is a highly stable optical instrument designed to restore most of the Hubble Space Telescope's (HST) scientific instruments to about 80% of their intended imaging capability. The correction involves positioning 2 mirrors in front of each of three scientific instruments; the Goddard High Resolution Spectrograph (GHRS), the Faint Object Spectrometer (FOS), and the Faint Object Camera (FOC). These mirrors will be remotely deployed with 6 mechanisms mounted to a Deployable Optical Bench (DOB), which extends into the hub area of the HST. Astronauts will replace the High Speed Photometer (HSP) instrument with the COSTAR instrument in one of the HST's axial bays during a repair mission scheduled for late 1993 or early 1994. Each of the mirror pairs will be adjusted on-orbit from the ground over a period of 45 days to achieve optimum image quality. Once adjusted these mirror pairs will remain fixed until the next adjustment period (estimated 6 months). The COSTAR instrument with the DOB and mirrors deployed is shown in Fig. 1.

Figure 1 COSTAR Instrument with DOB Deployed

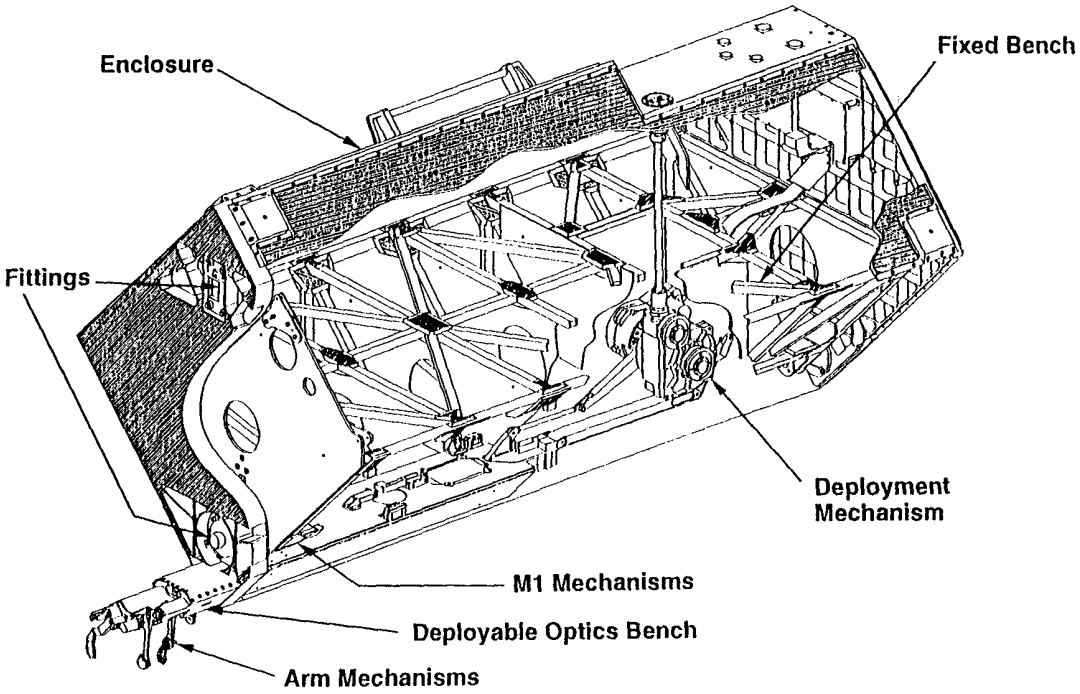

2. REQUIREMENTS

The design of the DOB was driven primarily by three factors: stability, envelope, and interfaces. The stability issues established the bench materials while the envelope determined its shape. Interfaces to the mirror mechanisms, electronics, and deployment system further constrained the design.

2.1 Optical stability

Optical Stability is divided into two time domains: short term stability (≤ 25 min exposure time) and long term stability (up to 4 months). The short term line of sight (LOS) stability requirement is 9 milli-arc-sec, while the long term LOS stability requirement is 410 milli-arc-sec.

2.1.1 Short term stability

Short term stability affects image quality due to thermal distortions resulting in mis-alignments of mirror pairs. These thermal distortions would be the results of thermal gradients across the structure due to un-even changes in the thermal environment of the hub area of the HST. Thermal modeling of the DOB predicted maximum side to side gradients to be less than 0.6°C which would seem to be insignificant. However, when trying to maintain less than a 9 milli-arc-sec LOS shift, most materials had coefficients of thermal expansion (CTE) producing unacceptable distortions when modeled with the DOB finite element structural model. A composite material of graphite epoxy was chosen as the major structural component of the DOB due to it's low CTE values (see comparison chart Table I).

Also affecting image quality is short term LOS jitter, which is a result of external vibration disturbances transmitted across the COSTAR instrument mounting interface. A deployed system goal of 50Hz minimum resonant frequency was imposed to minimize deflections due to vibrational disturbances. A minimum resonant frequency of 100Hz was established as a goal for the DOB structure in an effort to insure meeting the system 50Hz goal. Operational vibration (jitter) stability and thermal stability generated the derived requirements for the DOB of light weight, high stiffness, and very low CTE as summarized in Table I. Steel, titanium, and aluminum all have similar values for specific stiffness. High CTE values eliminated these materials for the DOB. Light weight and greater stiffness could be obtained from beryllium, but again the CTE was too high. Invar is a material with a very low CTE but Invar is a heavy material with a low specific stiffness. The only material choice for the DOB was graphite epoxy.

Table I Material Properties

Material	CTE $\mu\varepsilon$/ F	ρ lbs/in^3	E_t MSI	E/ρ
6061 Aluminum	12.7	0.10	10	100
416 Stainless	6.5	0.28	29	104
6Al-4V titanium	4.9	0.16	16.5	103
I-70 Beryllium	6.4	0.067	42	627
Invar 36	0.5	0.291	21.5	74
graphite epoxy	<0.15	0.064	20	312

2.1.2 Long term stability

Long term stability affects acquisition due to LOS drift and image quality due to alignment drift. This requirement is over a much longer time frame and therefore must take into account affects of moisture desorbtion in addition to the factors affecting short term stability. This demanded a close look at the coefficient of moisture expansion (CME) for the graphite epoxy composite laminate design. The scenario for distortion due to CME would be allowing the structure to absorb moisture while on the ground, then the structure would desorb over time in the vacuum of deep space after final alignment. The affect of CME can be analyzed by first calculating the amount of moisture absorbed given specific boundary conditions over a specific time period, then calculating the amount of time required to desorb that amount of moisture given specific boundary conditions and desorbtion rate. Then using the CME for the material, contractions of the material could be calculated over that time period or some shorter time period if necessary based on percentage of moisture lost.

2.2 Envelope

The DOB had very stringent envelope constraints defined by the HST existing design. Since the DOB would be deployed from an instrument installed in one of the HST's axial bays into the hub area, it would occupy a small triangular space between two other instruments and the fine guidance mirrors. This area is shown in Fig. 2, which is a view of the HST looking aft into the hub area. In addition to deploying under the Fine guidance mirrors, the DOB must also clear the "A" fitting which is one of the mounting fittings for the COSTAR instrument. The length envelope was not particularly demanding since it could use much of the available length of the instrument itself, which is approximately 86 inches long. This envelope would need to also accommodate the mirror arm mechanisms and deployment mechanism in it's stowed position which reduces the length of the DOB to 53.29 inches.

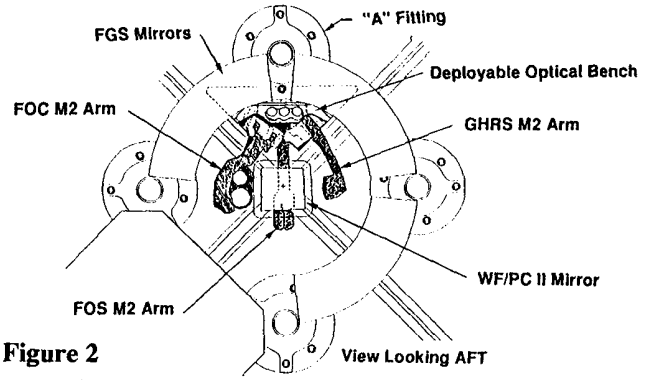

Figure 2

2.3 Interfaces

The DOB is a mounting platform for the 6 mirror mechanisms as described earlier, which are broken up into two categories: deployable arms and adjustable mechanisms. The arm mechanisms all require a mounting surface, access to deploy the arm, three threaded mounting holes and two pins to make the interface repeatable after assembly. The adjustable mechanisms are mounted internally, and need the same mounting surfaces, threaded holes and pins. In addition to these, the DOB interfaces to a set of 7 rollers for deployment, a deployment bracket, and electronics box.

3. STRUCTURE DESIGN

The DOB is primarily a graphite epoxy structure, developing most of it's strength from it's .160 inch thick skin. The basic construction shape is described in Fig. 3 shown with the removeable cover and aft skin removed. The structure is fully bonded using Hysol EA9394 and designed so that all joints are lap joints and no butt joints. This allows for larger bond surface area.

Figure 3 DOB Structure with Cover & Aft Skin Removed

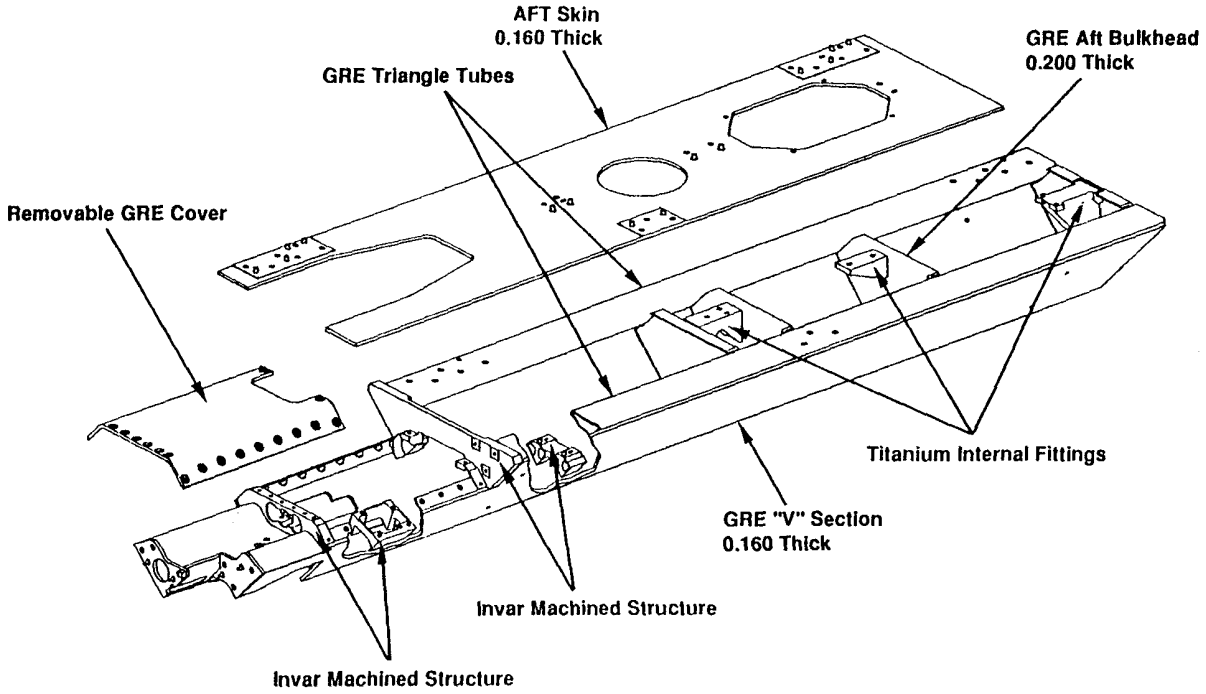

3.1 "V" section

The DOB is basically a triangular tube as shown in Fig. 4, with bulkheads located at each major load area to stiffen the skin in the area. These also help to control torsion in the main structure. The forward end of the DOB must reduce in size twice to fit within the envelope as described above, making two transitions necessary. The lower panels were formed as a single lay-up to maintain stiffnessthrough these areas. This "V" section is the key to maintaining the shape and integrity of the DOB. It was critical that this panel be fabricated with minimal twist or warp, since it formed the primary structure. This panel was then machined to its final shape including precisely located tooling holes, which indexed the part into the assembly fixture. All of the subsequent assembling would then be built on this foundation. The "V" section is joined to the aft skin with composite wound triangular tubes which completes the triangle cross-section. These tubes have a wall thickness of .080 inch thick. All of the other skins of the DOB are also .160 inch thick composite lay-ups.

Figure 4

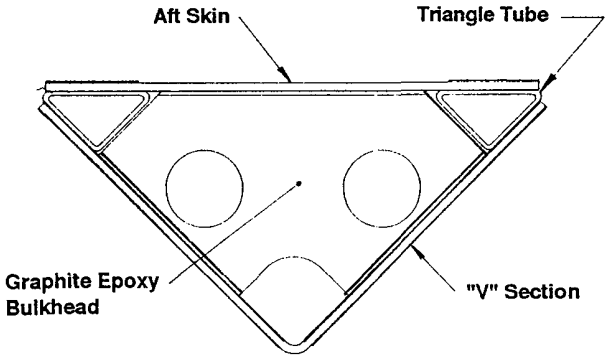

3.2 Bond joints

As mentioned above, all of the bond joints are lap joints. Besides providing larger bond surface area, this also makes it possible to match the CTE of the materials bonded since the CTE through the thickness of a graphite epoxy lay-up is orders of magnitude larger than the CTE in the plane of the laminate. To provide this bond area for the bulkheads which are .200 inch thick, plys were dropped in the center, then the outer two .040 inch ply sets were formed over 90° angle to form a .080 inch bond tab. This technique was used to make most of the right angle bond joints. This is shown in Fig. 5. Where this wasn't possible, 90° .040 or .080 inch thick bond composite angles were used.

Figure 5

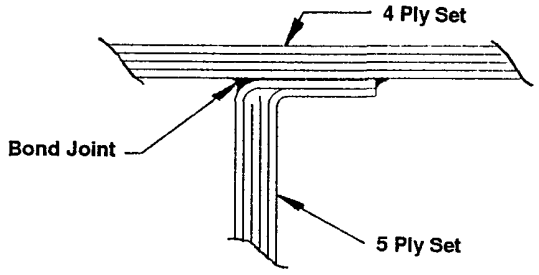

3.3 Machined fittings/mounts

In some areas such as the transitions that were mentioned above, it was necessary to include metallic machinings where the geometry required the CTE to be 3-dimensional. For these applications Invar was chosen to closely match the CTE of the graphite epoxy over relatively short spans. These machined fittings were also used where mounting of some of the mechanisms required pads, pins, and threaded holes in close proximity to one another. Where threaded holes or pins were required in graphite epoxy skins or bulkheads, titanium inserts were bonded into the material as shown in Fig.6. where the insert has a 124° countersink head so that as the mounting screw is torqued down, it puts part of the insert bond in compression. This philosophy of putting mounting bonds in compression is used in other mounting applications such as where machined fittings are bonded under skins thereby compressing the bond when mounting screws are torqued down. Nut plates also installed inside the triangle tubes as shown in Fig. 7, which also puts the bonded joint there in compression.

Figure 6

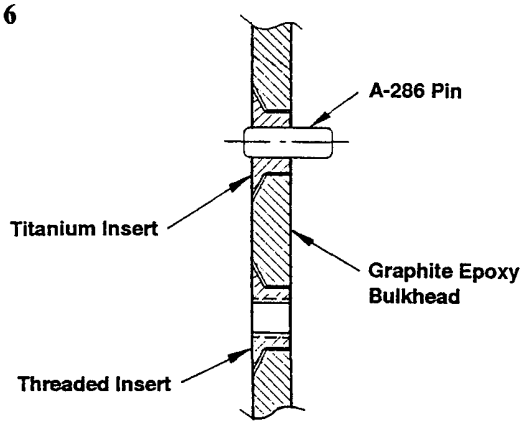

3.4 Removeable cover

The middle transition section of the DOB houses a large

complex mirror arm mechanism. Unlike all of the other mechanisms there wasn't sufficient clearance to install this mechanism into an existing opening. This drove the design to include a removeable structural cover. As most designers are aware, structural covers are difficult to implement and typically require some sort of pinning. Since this cover was in a graphite epoxy structure and needed to be flush, it posed additional problems. To fabricate a "pinned" assembly, a match-bonded assembly was designed which works like a match drilled assembly.

Figure 7

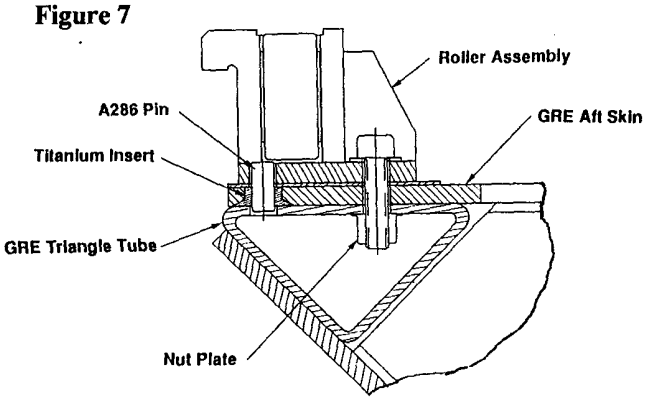

The key element in this removeable cover concept is a double countersunk centering sleeve. This sleeve has a close tolerance hole and 100° countersink that indexes off a countersunk screw. The outside diameter has a 124° countersink profile which is bonded into an oversized 124° countersunk hole in the graphite epoxy cover. This is shown in Fig. 8. The mid-cover assembly is assembled, and screws torqued while the adhesive is wet. In doing this the centering sleeve is free to move relative to the cover so that it can be assembled with reasonable tolerances and becomes a matched fit assembly when cured.

Figure 8 Removeable Cover

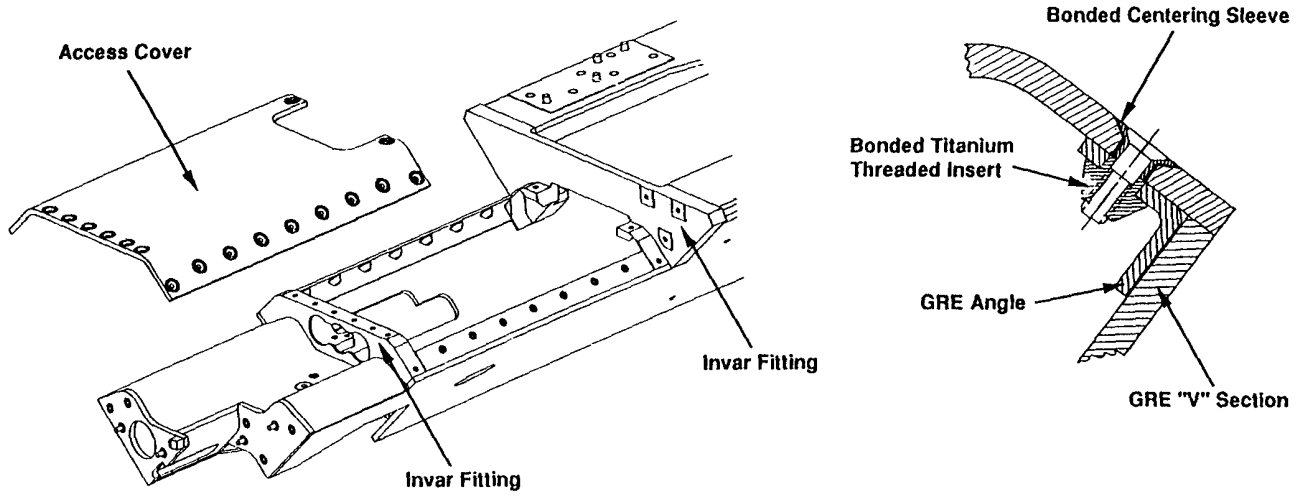

3.5 Electronics box mount

Three of the adjustable mechanisms in the DOB send signals to preamplifier electronics which need to be mounted on the aft end of the structure. Due to the thermal sensitivity of the DOB, the electronics box had to be thermally isolated from the DOB, since the electronics are a heat source. The box also needed a mount that would not induce strain into the structure from a mis-match in CTE between the aluminum electronics box and the graphite epoxy structure. To accommodate this, the box was mounted on four titanium flexures as shown in Fig. 9. These flexures allow the electronics box to expand relative to the DOB reducing the strain at its interface, while restraining the electronics box in position. The titanium material used reduces the heat transfer through conduction and provides adequate strength.

Figure 9

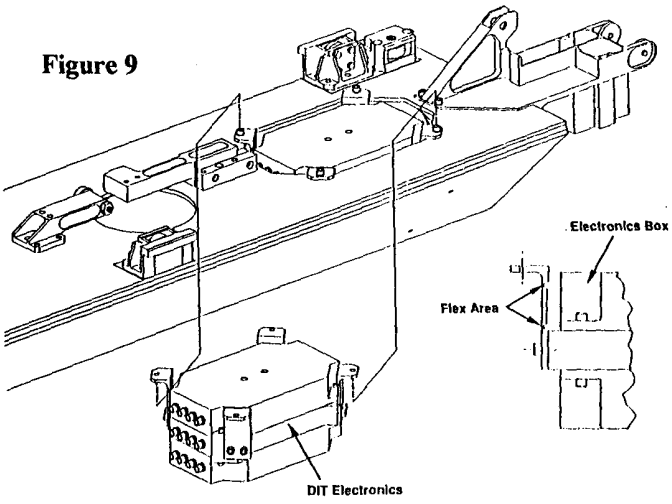

4. GRAPHITE/EPOXY COMPOSITE MATERIAL

As discussed earlier, it was necessary to use a material with low CTE properties to reduce any distortion due to potential thermal gradients in the structure due to uneven thermal conditions. Since graphite epoxy is a composite, it is possible to optimize the actual fiber selection and laminate design to achieve a balance between minimum CTE and maximum modulus of elasticity since material stiffness is also a concern. Thus a trade must be made in the laminate design process to select the lay-up and fiber with the optimum balance between the two.

Early in the design phase Hercules Aerospace in Salt Lake City, Utah was selected as the vendor to fabricate the DOB and a graphite epoxy truss also in COSTAR, having had experience building a similar truss in the GHRS instrument for Ball Aerospace earlier. Hercules was responsible for the laminate design and fabrication of the DOB and performed the analysis necessary to predict the properties used in the material trades.

4.1 Laminate design

The 3501-6 epoxy resin was chosen based on successful history on past programs and because there was a large data base of information with most fibers under consideration. Fiber lamina data was examined (see Table II) to determine which fibers would be the best choices for the DOB. Lamina data doesn't tell the whole story, however, since this is from uni-directional lay-ups where composite ply angles are not a factor. This data is used to select fiber and is used in the laminate design analysis program. As a result of this trade, a hybrid laminate using AS4 & HMS1 for the two triangular tubes based mainly on past history with the GHRS truss. The fiber chosen for the rest of the skin material was UHM. The selection was made based on it having the highest modulus of elasticity with past flight history. The GY70, P-75 &P-100 fibers were not chosen because there was very little data and no flight history available.

Table II Room Temperature Lamina Properties

		Fibers with 3501-6 Epoxy Resin							
Property	**Units**	AS4	UM6	HM7	HMS1	UHM	GY70	P-75	P-100
E_{xt}	MSI	**20.7**	22.8	24.0	**30.0**	**38.5**	40.6	44.1	58.4
E_{xc}	MSI	**20.2**	21.6	22.0	**26.5**	**36.0**	36.0	35.7	54.2
E_{yt}	MSI	**1.35**	1.38	1.38	**1.12**	**1.27**	1.00	0.87	-
E_{yc}	MSI	**1.35**	1.38	1.38	**1.15**	**1.50**	0.87	0.87	-
G_x	MSI	**0.71**	0.83	0.83	**0.84**	**0.78**	0.59	0.58	0.81
G_y	MSI	**0.50**	0.50	0.50	**0.42**	**0.49**	0.50	0.33	-
α_x	με/°F	**-.035**	-0.22	-0.22	**-0.33**	**-0.45**	-0.45	-0.67	-
α_y	με/°F	**11.8**	12.0	12.0	**14.9**	**13.6**	15.2	15.2	-

x = longitudinal ply direction, y = transverse ply direction,
E_t = tensile modulus of elasticity, E_c = compressive modulus of elasticity, G = shear modulus of elasticity, α = CTE

Using this lamina data a number of composite ply lay-up designs were analyzed for both the tubes and the skin material. The tube design was baselined quickly since there was really only a concern with optimizing the CTE in the longitudinal direction of the tube along with having a high tensile modulus of elasticity. The tube lay-up chosen was 68% HMS1 0° plies (0.0069 in thick), 32% AS4 ±70° plies (0.0033 in thick), with a fiber volume of 62%. The skin material was a little more difficult to baseline. The ideal laminate would have a very high modulus of elasticity while having a low CTE in both longitudinal and transverse skin directions. The UHM fiber was already selected and a quasi-isotropic lay-up using 0° plies and ±45° plies would produce a lay-up with close to zero CTE in both directions, however the modulus would only be around 13.4 MSI. The modulus could be increased by increasing the 45° ply angle but this would come at the cost of an unbalanced CTE values in the longitudinal and transverse directions. Several of these combinations were run in the DOB finite element structural model to determine the acceptable limits that could be tolerated. The resulting laminate chosen was 50% 0° plies (0.0049 in thick), 50% ±79° plies (0.0049 in thick), with a fiber volume of 65%. The predicted laminate properties are listed in Table III.

Table III Predicted Laminate Properties

Component	Material	Fiber Volume %	E_{xt} MSI	E_{yt} MSI	α_x με/°F	α_y με/°F
Triangle Tube	HMS1/AS 4	62	19.8	-	-0.009	-
DOB Skins	UHM	65	20.0	18.5	-0.023	0.085

4.2 CTE testing

Graphite epoxy laminate design and fabrication has been refined over the years so that the above properties are very predictable. These studies do show, however, that subtle changes in ply angle, fiber volume,and other manufacturing processes significantly effect CTE and have subtle effects on other properties. This necessitates CTE testing during both development of the material and production of the flight components. Reviewing the anticipated CTE values, it becomes obvious that measuring samples or actual parts in this low range becomes quite difficult. Several companies have spent many years developing test methods for measuring CTE's in this range trying to get accuracies below ±.1με/°F. Entire papers could be written and have been on this subject. Eastman Kodak Co. in Rochester, NY has done extensive analysis to support their test facility's "standard uncertainty" of better than 0.02με/°F. This was the basis for deciding to test samples at their facility.

4.3 Development testing

Test panels and tubes were prepared with slightly different ply angles and fiber volume for each of the two laminate types. These were cut into 3 samples each for testing at Kodak so that an optimum ply angle and fiber volume could be chosen. After reviewing the results (Table IV), it was discovered that fiber volume was more critical than initially expected, requiring that the nominal value be 67% controlled to within ±1%. The ply angle certainly had an effect on CTE but was not sensitive under a degree or two and can be controlled well within that range. Controlling fiber volume has proved to be more difficult but techniques have been developed to reduce the potential scrap rate to a handful of parts. A similar process was followed in proving the tube laminate design. After the development testing was over, a tolerance for the laminate CTE properties was defined for the DOB Specification. Meeting the CTE tolerance would be the acceptance criteria for the components used in the DOB. The DOB skin laminate longitudinal CTE requirement is α_x=0.01±.05με/°F and the transverse CTE requirement is α_y=0.07±.05με/°F. The DOB triangle tube laminate CTE requirement is α_x=0.0±.05με/°F.

Table IV Development Testing Results

Sample/ Ply Angle/ Direction	Fiber Vol %	Ply Angle	α_x με/ F	α_y με/ F
135-75-90-1K	64.2	75	-	0.212
135-75-90-2K	64.2	75	-	0.215
135-75-0-1K	65.7	75	0.024	-
135-77-90-1K	63.8	77	-	0.172
135-77-0-1K	65.8	77	0.051	-
135-77-90-2K	64.6	77	-	0.193
135-77-0-2K	63.8	77	0.053	-
135-77-90-3K	67.0	77	-	0.093
135-77-0-3K	63.8	77	0.063	-
135-79-90-1K	63.4	79	-	0.145
135-79-0-1K	**65.8**	**79**	**0.050**	**-**
135-79-90-2K	64.2	79	-	0.148
135-79-0-2K	64.2	79	0.059	-
135-79-90-3K	**67.5**	**79**	**-**	**0.067**
135-79-0-3K	63.4	79	0.073	-

4.4 Component CTE Results

Using the information from the development testing, both the tube and skin laminates were optimized and components were fabricated for the DOB development unit. The components were built oversize to allow samples to be cut and tested for actual CTE values. The test results for the major components of the DOB are shown in Table V. All CTE for these samples came within the specification tolerance values. The data shows that the longitudinal CTE values tended to be closer to 0 than did the transverse CTE values.

Table V Actual Laminate Properties

Component	Fiber Vol %	α_x με/ F	α_y με/ F
Triangle Tube 1	60.6	-0.013	-
Triangle Tube 2	62.9	-0.020	-
"V" Section	66.3	0.053	0.116
Aft Bulkheads	69.5	0.053	0.103
Aft Skin	68.1	0.003	0.088
Mid Cover	68.8	0.000	0.131
Forward Skin	68.7	0.002	0.002

4.5 CME Considerations

Graphite epoxy is known to be a slightly hygroscopic material and can tend to expand as a function of moisture content. This expansion is quantified with a coefficient of moisture expansion (CME). Graphite epoxy laminates can be optimized to minimize CME. However, this sometimes comes at a cost of not having an optimized CTE laminate. Since CME has an effect which occurs over a longer period of time than the effects of CTE, it tends to have a larger effect on long term LOS stability rather than short term stability. Distortions in the DOB come from its lack of symmetry in relation to it's mounts. An analysis of the DOB was made to determine the amount of moisture would be absorbed over a 6 month period when exposed to 50% relative humidity. The analysis aslso examined the effect of the moisture on the DOB. The linear expansion rate depends on both CME and the diffusion rate. The values for CME (β) were supplied by Hercules Aerospace from historical data for the materials used in the DOB. The values used for the diffusion constant for the graphite epoxy (D), component thickness (d) and saturated moisture content (C_s) are shown in Table 6. The results of this analysis showed a "roll" angle at the mirror locations of 4 arc-sec which is well within the 15 arc-sec acceptable limit from an earlier sensitivity analysis.

Table VI Moisture Properties

Material	UHM	HMS/ AS4
β ($\mu\varepsilon/\%H_2O$)	270	80
D (min^2/day)	2.2	3.7
C_s ($\%H_2O$)	0.45	0.68
d (inch)	0.16	0.08

5. INVAR & TITANIUM MACHININGS

As mentioned earlier, metallic machinings were required in the design mainly for mounting purposes. In the forward end, where thermal distortion causes the most effect on mirror motions, it was necessary to use a material with a low CTE to be close to that of the graphite epoxy. Invar 36 was used for these machinings. In the aft end of the DOB, where the bench is mounted to it's rollers, additional machinings were needed to provide mounting interfaces for the DOB and are internal to the graphite epoxy skins. These machinings were relatively small, were not primary structure, and did not have appreciable effect on thermal distortion of the DOB. Titanium was used for these.

5.2 Invar CTE properties

Many studies have been done on Invar in an effort to drive it's CTE to zero. There are basically two Invar alloys used for these purposes: Invar "36" and "Super" Invar. "Super" Invar is known to have very low CTE properties (0.1 $\mu\varepsilon/°F$) but has been known to have stability problems due to a low temperature transformation. Invar "36," in its annealed condition, has a CTE of 0.7 $\mu\varepsilon/°F$ which is significantly lower than most other metals. Its CTE can be reduced further by either cold working, heat treating or both. These techniques can produce some unwanted side effects such as micro-creep and lowered micro yield properties. The approach taken with the Invar used in the DOB was to heat treat Invar "36", followed by thermally treating the material after quenching. This would produce a CTE of less than 0.5 $\mu\varepsilon/°F$ while maintaining stable mechanical properties.

6. STRUCTURAL ANALYSIS

During the detailed design and optimization of the DOB, finite element analysis was used to provide the necessary level of accuracy to support the mechanical design. The detailed finite element modeling and post processing was performed using the SDRC SUPERTAB Computer Aided Engineering System (IDEAS version VI) from General Electric CAE International. Structural (stress and dynamics) solutions were obtained using MSC/NASTRAN, a large scale general purpose finite element computer program supported by the McNeal -Schwindler Corporation. NASTRAN was run on a VAX 8600 computer.

6.1 Design Optimization

The structural design and analysis is one part of the overall performance analysis. Thermal analysis, optical design and analysis, and LOS error budget analysis all combine with the structural design to define the final preformance. In all cases, structural analysis, using the detailed mechanical design, takes the operational disturbances, thermal and vibrational, long and short term, and provides the operational structural distortions to optical analysts for LOS determination. The resulting optical

LOS deviation is evaluated as part of the overall instrument error budget. Design iterations are performed on the design to insure the preformance requirements are achieved.

Structural analysis of the graphite epoxy DOB has been integrated into the laminate design and optimization process. A NASTRAN finite element structural model of the DOB which included over 500 grids and 700 elements was developed for use in the optimization of the design.

During the optimization of the material properties, temperature profiles were input to the DOB NASTRAN finite element model for thermal distortion analysis. LOS ray traces were performed using the distorted optics geometry that resulted from the temperature gradients. From this analysis it was determined that the GRE CTE (including measurement tolerance) could range between ±0.17 με/°F to meet the error budget. This distortion analysis also demonstrated that Invar fittings could be used with the GRE. The evolving GRE modulous of elasticity was continously evaluated using NASTRAN normal modes analysis to insure that the 100 Hz. stiffness requirement would be achieved by the DOB structure.

Prior to the development of the detailed structural model, a 10 element beam model was used to validate the design concept, determine support points for optimum stiffness, and to determine the necessary material properties and thickness to meet stiffness requirements. Sufficient detail was then included in the current structural model so that it could be used as the final stress and dynamics analysis model with necessary modifications as the design matured. This model was used alone to support mechanical design trade studies as well as being incorporated into the full COSTAR instrument model for launch load and on-orbit jitter analysis.

6.2 Structural Model

Sufficient detail was included in the structural model so that it could be used in the dynamics, thermal distortion, and final stress analyses. A total of 549 grid points were used to describe the geometry. A total of 686 plate elements (CQUAD4 and CTRIA3) form the tubular surface and 23 CBAR elements were used to define the reinforcing tubes. The total structural model weight was 15 pounds with an additional 30 pounds of optical components, mechanisms, and deployment hardware. The test configuration for the model weighed 36.6 pounds which was broken down as 20.48 pounds for dummy masses, 1.68 pounds for accelerometers, and a structural weight of 14.41 pounds. The actual test structure weighed in at 14.95 pounds. The numerous cut-outs for light paths and mirror deployment clearances were included in the structural model. Figure 10 shows the finite element structural model.

Figure 10 COSTAR DOB Finite Element Structural Model

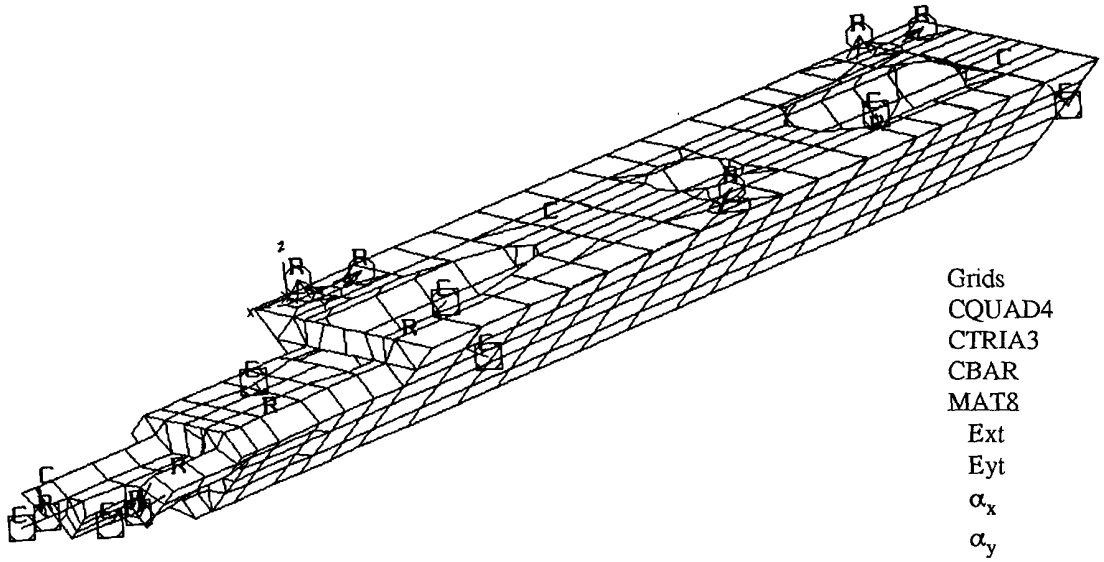

Grids	549
CQUAD4	562
CTRIA3	122
CBAR	23
MAT8	
Ext	18.9 Msi
Eyt	15.1 Msi
α_x	-.17 με/°F
α_y	+.17 με/°F
Weight	36.6 lb

The GRE plate material modulus of elasticity used for analysis in the structural model was E_{xt}=18.9 Msi and E_{yt}=15.1 Msi. These values are slightly less than the final measured tensile modulus values since the final material iteration was not completed at the time of the analysis. This provides for some modeling conservatism. The NASTRAN plate elements were considered as orthotropic, using the MAT8 material data input. The material properties were obtained from the GRE supplier and bench fabricator and agreed well with results from PCLAM and NASTRAN PCOMP analysis for individual layers and orientations.

Dynamic characterization of the structure was performed by NASTRAN normal modes analysis. Normal modes analysis included both LANCZOS and modified Givens methods for eigenvector extraction. Thermal distortion statics load cases were used to establish the DOB thermal stability.

7. STRUCTURAL VERIFICATION

The design was optimized for CTE and structural rigidity. Of these, structural stiffness provided the best means for early design verification. The structural finite element model was verified by vibration testing on a 30000 pound force shaker. Modal survey test data were obtained from 3-axis random vibration. Test mode shapes were determined using a Gen Rad 2508 8 channel system with SDRC Modal Plus software. Test resonances and mode shapes were compared with analysis results. Analysis results were obtained using MSC NASTRAN. NASTRAN normal modes analysis included both LANCZOS and modified Givens methods for eigenvector extraction.

7.1 Vibration test Description

Modal survey test data was obtained from 3-axis random vibration flat spectrum of 0.0005 g^2/Hz from 20 to 500 Hz. Ten accelerometer positions along the length of the structure, with a total of 22 single axis accelerometers, were used to obtain data for the frequency and mode shape determination. Figure 11 shows the orientation and numbering for the accelerometers. Also shown in Figure 11 are coordinate axes. Accelerometer position numbers start at the back of the DOB with No. 1 and proceed to the front free end No. 9. Accelerometer locations 10, 11, and 12 were fixture and test control accelerometers. No. 13 was located near the front free end on the +y side on the GHRS dummy mass at approximately the same axial location as No.8. Accelerometer No. 9 was located on the front free end on the -y side on the FOC M2 dummy mass. Axial (X-axis) data was not expected to provide much information so several accelerometer locations did not have X data accelerometers. Data 7x, 8x, and 13x were estimated from data 9x for mode shape determination.

Figure 11 DOB Vibration Test Data Accelerometer Locations

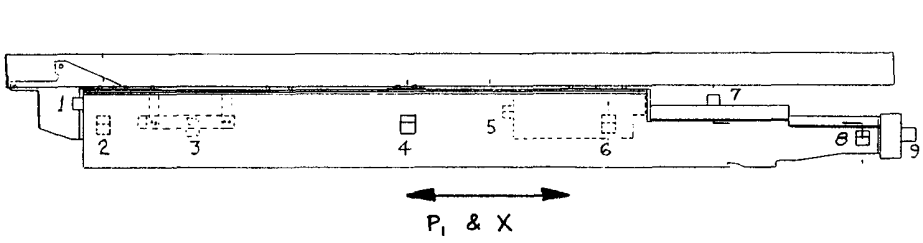

LOCATION	DATA AXES
1	X
2	Y, Z
3	X, Y, Z
4	Y, Z
5	X, Y, Z
6	Y, Z
7	Y, Z
8	Y, Z
9	X, Y, Z
13	Y, Z

The random vibration test data from all three axes were reduced and transfer function plots were generated. The mode shapes were extracted from the data sets which best indicated each mode. The DOB finite element model was modified to represent the vibration test configuration and NASTRAN normal modes analysis was performed to be compared with the test results. Tables of normalized displacements for each accelerometer position were compared for test and analysis results.

7.2 Structural Test and Analysis Results

Table VII gives a list of the modes, a brief description of the mode shape, and compares the test results with the analysis results. Also included in Table VII is the percent deviation of analysis predicted results from the actual test values. Tables VIII thru X compare the test and analysis mode shapes for the accelerometer locations. In these tables the test eigenvector is compared with the finite element model eigenvector for each eigenvalue. The test eigenvector has been normalized to the maximum deflection. The corresponding analysis eigenvector has been normalized to the analysis deflection that occurred at the same location and degree of freedom as in test.

Table VII Test/Analysis Resonance Comparison

MODE No.	TEST FREQ. (Hz.)	ANAL. FREQ. (Hz.)	% DIFF	DESCRIPTION
1	98.8	104.5	5.8%	First Z-axis bending mode of free end
2	161.8	166.3	2.8%	First Y-axis bending mode of free end
3	189.3	-	-	Torsional mode of free end
4	246.9	247.6	0.3%	Torsional mode of full length
5	299.0	282.4	-5.9%	Second Z-axis bending mode of free end
6	305.8	-	-	Torsion- free end and electronics out of phase
7	310.1	-	-	Z-axis electronics box mode
8	312.0	-	-	X-axis of FOS/GHRS M1 mechanism mass
9	360.6	348.9	-3.4%	Second Y-axis bending with main body
10	423.9	435.2	2.7%	Third Z-axis bending including main body
11	495.6	469.9	-5.5%	Higher order Z-axis (bending of main body)

The structure fundamental resonance was measured to be 98.8 Hz. The mode shape is Z-axis beam bending. The analysis determined fundamental resonance is 104.5 Hz, 5.8% above the measured value. The comparison of the mode shape in Table VIII shows agreement between the measured and predicted shapes.

Figure 12 Mode 1 - Analysis Results

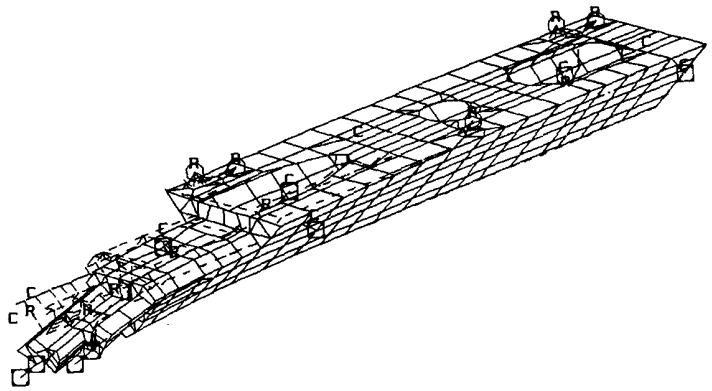

Table VIII Mode 1 Test/Analysis Shape Comparison

	Test	f=99	Hz	Anal	f=105	Hz
No	X	Y	Z	X	Y	Z
1	.001	-	-	.003	0.0	0.0
2	-	-.009	-.024	.003	.002	-.004
3	-.004	-.005	-.006	.001	.000	-.005
4	-	.011	-.003	.006	.010	-.025
5	-.011	-.009	.0371	-.017	-.003	.040
6	-	.026	.122	.002	.015	.114
7	.014	.002	.357	-.030	.019	.189
8	.028	.053	.708	.074	.051	.712
13	.028	.078	.803	.066	.049	.752
9	.039	.032	1.000	.091	.076	1.000

The second primary resonance was Y-axis beam bending measured at 161.8 Hz. The analysis predicted this resonance to be 166.3 Hz, 2.8% above the measured value. The analysis mode shape showed significant Z-direction component, not the nearly pure Y-axis bending as measured.

Figure 13 Mode 2 - Analysis Results

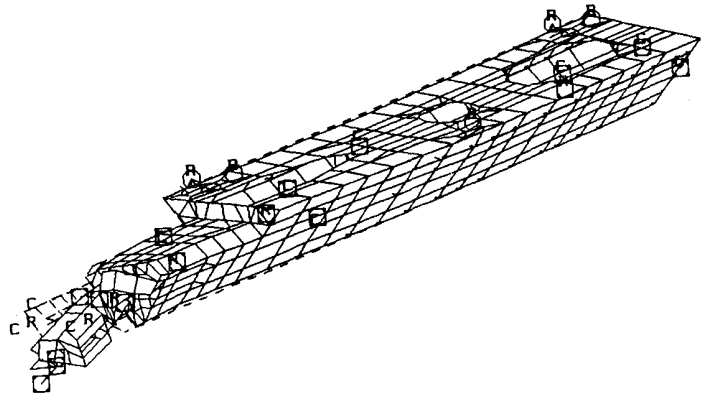

Table IX Mode 2 Test/Analysis Shape Comparison

	Test	f=162	Hz	Anal	f=166	Hz
No	X	Y	Z	X	Y	Z
1	.004	-	-	.007	0.0	0.0
2	-	-.018	-.023	.005	.030	.120
3	.0003	-.026	-.009	.003	.016	.049
4	-	.027	-.026	.017	.058	-.085
5	.0003	.057	.080	-.005	-.054	.245
6	-	.119	.157	-.010	.124	.588
7	.014	.243	-.007	.004	.117	.426
8	.029	1.000	-.535	-.192	1.000	-2.24
13	.029	.707	.084	.215	1.164	-2.20
9	.041	.809	-.391	-.273	1.124	-2.10

An additional Y-axis bending mode was measured at 189.3 Hz. This mode shape showed slightly different motion of the dummy mass at the end. This could be an indication of compliance associated with the attachment of the dummy mass to the DOB which was not considered in the analysis.

The fourth measured mode was beam torsion at 246.7 Hz. The analysis results for this mode was 247.7, only .4% over the measured value. The test and analysis mode shapes, compared in Table X, show similar profiles.

Figure 14 Mode 4 - Analysis Results

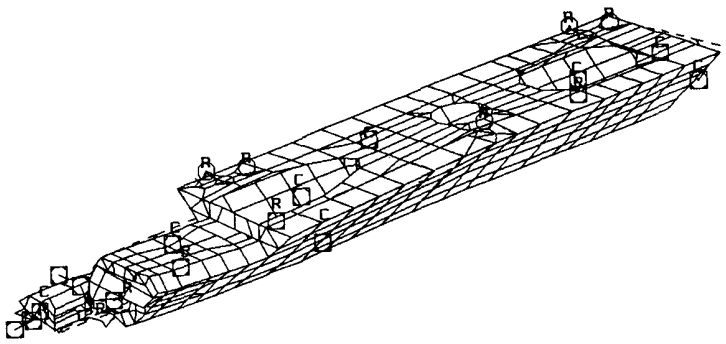

TABLE X Mode 4 - Test/Analysis Shape Comparison

	Test	f=247	Hz	Anal	f=248	Hz
No	X	Y	Z	X	Y	Z
1	.002	-	-	.020	0.0	0.0
2	-	.042	.143	.019	.122	.634
3	-.017	.166	.091	.010	.090	.349
4	-	-.010	-.074	.046	.194	-.127
5	-.018	-.214	-.280	.049	-.060	.958
6	-	.027	-.469	-.070	.576	2.099
7	.064	.356	-.352	.095	.739	1.106
8	.130	.648	.116	.754	1.744	1.752
13	.130	.327	-.187	-1.10	1.791	-5.26
9	.183	.499	1.000	.426	2.359	1.000

This summarizes the primary beam modes of the DOB; Z-axis bending, Y-axis bending, and torsion. The only beam primary mode missing is axial resonance which is above the range of interest and was not obtained. Additional modes above these primary beam resonances are complex and difficult to interpret with the limited degrees of freedom from the test modal survey data. These higher order modes have been included in Table VII for reference.

7.3 Structural Test and Analysis Discussion

The finite element results presented here are from a math model which has not been adjusted in any way to match the test results. For primary structural modes, such as first and second beam bending modes, the test and analysis results are in agreement. The comparison between test and analysis is typical in that the analysis finite element model is slightly stiffer than the actual hardware. Comparison of test and analysis resonances show the finite element analysis to be accurate in the prediction of resonant frequency and mode shape for complex GRE structures using the analytically generated orthotropic material properties.

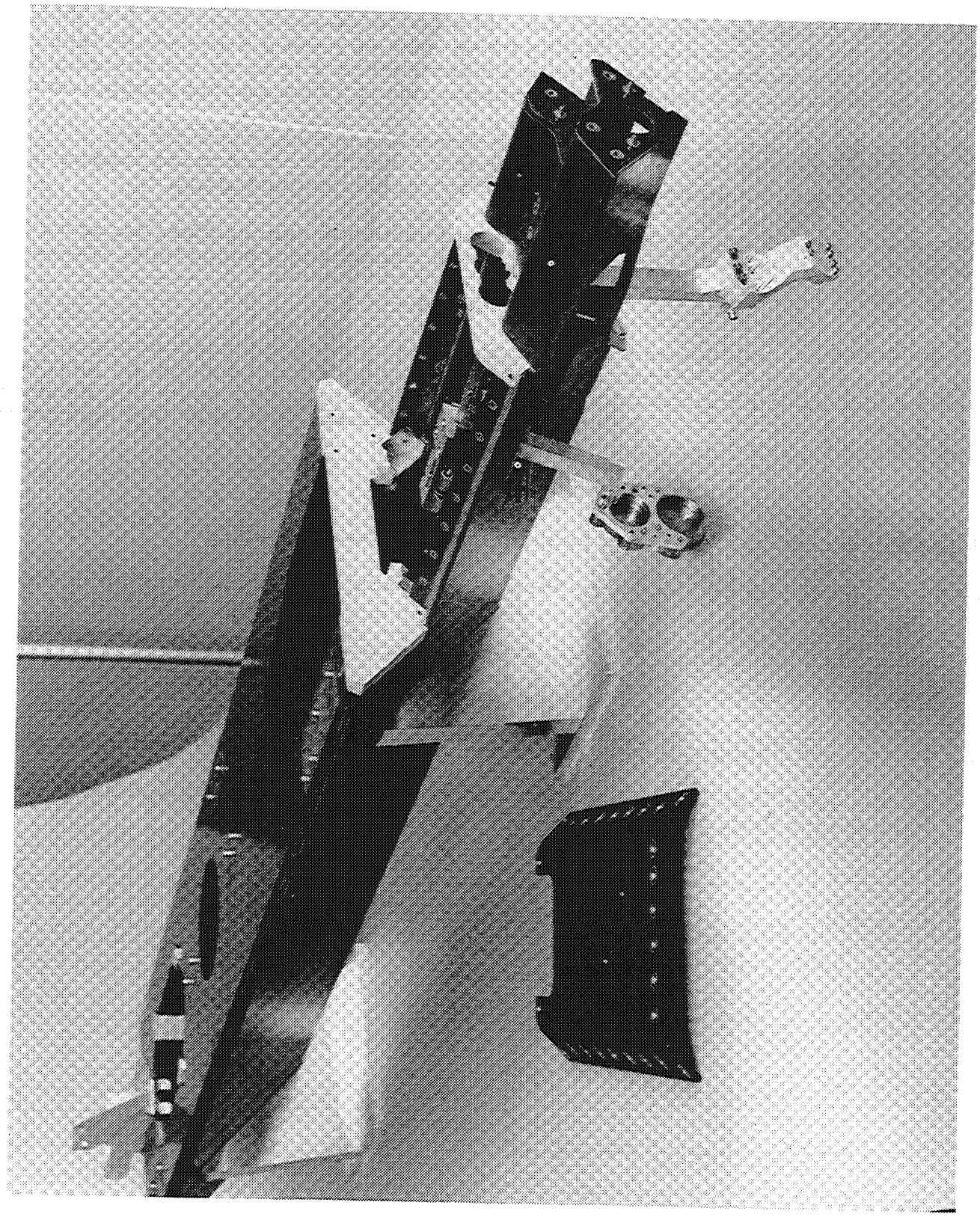

Figure 15. DOB Development Unit

For the more complex mode shapes, the agreement between test and analysis eigenvectors tended to be more difficult to establish. The primary reason for this is that test instrumentation was limited, and positioned to characterize the fundamental structure modes. Higher order, complex mode shapes could not be determined from the limited data. With the structural finite element model verified with the fundamental modes, the more complex modes are best determined from the analysis results.

Optical mechanism access dictated the use of a structural cover. Accelerometer No. 7 was located on this cover. In all cases the analysis predicted less motion of this accelerometer than was observed in test. This could indicate some compliance in the attachment of the structural cover. The fundamental resonances appear to not have been severely effected.

Some of the difficulties associated with the comparison of test and analysis mode shapes could have been reduced with othogonality checks on the eigenvectors. Orthogonality checks were not performed on the eigenvectors due to time limitations.

8. CONCLUSIONS

An ultra-low CTE structure can be designed with careful selection of specific graphite epoxy laminates and Invar parts. Use of orthotropic material properties, analytically determined graphite epoxy lay-up physical properties, and careful finite element modeling results in accurate prediction of the structure stiffness for complex GRE structures. It is necessary to combine precise CTE testing with the laminate design and the component fabrication process control. A photograph of the finished DOB development unit has been included as Fig. 15.

9. ACKNOWLEDGEMENTS

This work is funded in part by the NASA Goddard Space Flight Center under contract NAS5-36000.

We wish to thank the Hercules Aerospace Company for providing the necessary laminate experience and material property data.

We also wish to thank Nelson W. Smith, of Ball Aerospace for his help in the vibration data reduction analysis.

10. REFERENCES

1. C.W. Marschall and R.E. Maringer, "Dimensional Instability an Introduction," Battelle, Columbus Laboratories, Columbus, Ohio, Pergamon Press
2. Ball Aerospace Systems Group, "Graphite/Epoxy Desorbtion Effects on LOS and WFE," P.A. Lightsey, Dec 19,1991
3. Ball Aerospace Systems Group, "Invar in Graphite Epoxy Structures," D.C. Neam, Mar 15, 1991